American Mineralogist, Volume 92, pages 124–138, 2007

An evaluation of synthetic fluid inclusions for the purpose of trapping equilibrated, coexisting, immiscible fluid phases at magmatic conditions

ADAM C. SIMON,[1,*] MARK R. FRANK,[2] THOMAS PETTKE,[3] PHILIP A. CANDELA,[4] PHILIP M. PICCOLI,[4] CHRISTOPH A. HEINRICH,[3] AND MICHAEL GLASCOCK[5]

[1]Department of Geoscience, University of Nevada, Las Vegas, Nevada 89154-4010, U.S.A.
[2]Department of Geology and Environmental Geosciences, Davis Hall 312, Normal Road, Northern Illinois University, DeKalb, Illinois 60115, U.S.A.
[3]Isotope Geochemistry and Mineral Resources, Department of Earth Sciences, Federal Institute of Technology, ETH Zentrum NO, CH-8092, Zurich, Switzerland
[4]Laboratory for Mineral Deposits Research, Department of Geology, University of Maryland, College Park, Maryland 20742, U.S.A.
[5]Research Reactor Center, University of Missouri, Columbia, Missouri 65211, U.S.A.

ABSTRACT

We report data that allow us to evaluate the method of trapping immiscible, saline aqueous fluids (i.e., vapor and brine in the NaCl-KCl-HCl-$FeCl_2$-$AuHCl_2$-H_2O system) as synthetic fluid inclusions in pre-fractured quartz cores in order to quantify the concentrations of Au, Fe, K, and Na, among coexisting three-phase, immiscible fluids (i.e., haplogranite melt, brine, and vapor) at magmatic conditions. Coexisting vapor and brine were trapped experimentally at 800 °C and 100–110 MPa as synthetic fluid inclusions in both quartz microfractures and quenched silicate melt (i.e., glass), and also sampled indirectly using the recovered quenched aqueous fluid. Quartz-hosted and glass-hosted brine inclusions were analyzed by laser-ablation inductively-coupled-plasma mass spectrometry (LA-ICPMS) and instrumental neutron activation analysis (INAA), respectively. Quenched aqueous fluid from each experiment containing a quartz core was recovered and analyzed by atomic absorption spectrophotometry (AAS). The composition of aqueous fluids trapped as quartz-hosted inclusions, glass-hosted inclusions, and those recovered after quench yield consistent and precise data, at the 2σ uncertainty level, for the elements of interest. The overlapping Au, Fe, K, and Na concentrations in aqueous fluids trapped and analyzed via three entirely different instrumental techniques (i.e., LA-ICPMS, INAA, and AAS) suggest strongly that quartz microfractures heal on a slow enough time scale to permit entrapment of fully equilibrated aqueous fluids at our experimental *PTX* conditions. The data evince clearly that the chemical composition of fluids in quartz microfractures at the time of self-healing represents equilibrium conditions; hence, synthetic fluid inclusions in experiments with low thermal gradients across the charge provide a reasonable estimate of fluid composition at least at the experimental conditions examined in this study.

Keywords: Analysis (chemical), fluid inclusions, experimental petrology, magmatic-hydrothermal fluids, element partitioning, immiscible fluids, igneous petrology, vapor, brine

INTRODUCTION

Specialized micro-analytical techniques such as laser-ablation inductively-coupled-plasma mass spectrometry (LA-ICPMS), proton-induced-X-ray-emission (PIXE), and synchrotron X-ray fluorescence (SXRF) are being applied at an ever-increasing rate to quantify the compositions of natural, aqueous fluid inclusions of variable salinities, from geologic settings including ore deposits, subducted oceanic slabs, and metamorphic and sedimentary environments (e.g., Heinrich et al. 1992, 1999, 2003; Ryan et al. 1993, 2001; Shepherd and Chenery 1995; Mavrogenes et al. 1995; Günther et al. 1998; Audétat et al. 1998, 2000; Ulrich et al. 1999, 2001; Kamenetsky et al. 2002; Audétat and Pettke 2003; Pettke et al. 2003; Baker et al. 2004; Scambelluri et al. 2004a, 2004b; Gagnon et al. 2004; Klemm et al. 2004; Kostova et al. 2004; Allan et al. 2005; Hanley et al. 2005; Landtwing et al. 2005a, 2005b). However, our ability to comprehend the relationship between natural fluid inclusion data and the equilibria controlling element partitioning between melt(s), mineral(s), and aqueous and gaseous volatile phase(s) is severely limited owing to a dearth of experimental data that constrain thermodynamically the effects of pressure, temperature, acidity and salinity of the aqueous fluid(s), oxygen fugacity, sulfur fugacity, inter alia, on element distribution among coexisting, multi-phase, immiscible magmatic-hydrothermal aqueous, silicate, and sulfide fluids. Element mass transfer can occur by processes such as magmatic degassing, owing to decompression and/or crystallization of silicate melt, the concomitant mass transfer of elements from silicate and/or sulfide fluids into aqueous fluid(s), as well as by processes attending condensation and boiling of aqueous fluid(s) owing to changes in intensive and extensive parameters as the aqueous fluid(s) percolates through the magma body and surrounding country rock. Collection of these thermodynamic data is required to model and understand quantitatively how elements

* E-mail: adam.simon@unlv.edu

are redistributed within Earth's lithosphere.

Traditional laboratory experiments designed to quantify the solute loads of magmatic-hydrothermal fluids, defined herein to include aqueous fluids of any salinity, as a function of pressure-temperature-composition (*PTX*) have been historically confined to working in a one-phase fluid field (i.e., vapor, brine, or supercritical fluid) at magmatic temperature and pressures of no more than a few hundred MPa (Chou and Eugster 1977; Frantz and Popp 1979; Popp and Frantz 1980; Candela and Holland 1984; Whitney et al. 1985; Kovalenko et al. 1986; Korzhinskiy 1987; Wood et al. 1987; Hemley et al. 1992; Williams et al. 1995; Liu et al. 2000). In experiments with low-salinity fluids, the quenched fluid is extracted from the charge after termination of the experiment and analyzed at ambient conditions with the hypothesis that the solute load in the quenched fluid is equivalent to the solute load at the experimental *PTX* conditions. The ability to demonstrate that the quenched fluid does not suffer precipitate loss during quench is a fundamental requirement of this experimental design. This technique has not been applied at pressures above a few hundred MPa owing to the precipitation of solutes from the aqueous phase during quench, resulting in an underestimation of the elemental concentration of the solute. To determine experimentally the solute load of aqueous fluids at higher pressure, experiments traditionally have been performed in an aqueous fluid ± melt ± crystal(s) system and the solute composition of the single-phase aqueous fluid was calculated by mass difference of the initial and final crystal or melt (Anderson and Burnham 1965; Manning 1994; Manning and Boetcher 1994; Newton and Manning 2000, 2002). This method can yield accurate mineral solubilities owing to the ability to quantify masses with 1σ reproducibility down to 0.002 mg (Newton and Manning 2000). However, the mass-balance method of quantifying element partitioning between silicate melt and aqueous fluid can be problematic owing to crystallization of the melt upon quench in charges where only melt and aqueous fluid are loaded. This leads to difficulty in quantifying the melt chemistry and, thus, the ability to perform accurate mass-balance calculations.

Günther et al. (1998) tested the use of pre-fractured quartz (cf. Bodnar and Sterner 1985) to trap fluid inclusions in a single-phase region. Their study tested the accuracy of LA-ICPMS to quantify the solute load of individual, single-phase, quartz-hosted fluid inclusions. They loaded a pre-fractured quartz chip with an aqueous solution of known chemistry and equilibrated this assemblage at 660 °C and 152 MPa for 241 hours. Petrographic observation of polished quartz cores revealed fluid inclusions up to 100 μm in diameter trapped in self-healed microfractures. Their study demonstrates that accurate solute chemistry can be obtained by LA-ICPMS analysis of individual fluid inclusions, trapped in a one-phase field, by using microthermometrically determined Na concentrations of each fluid inclusion to convert element isotope ratios (i.e., Fe:Na) yielded by the mass spectrometer to absolute element concentrations.

The aforementioned experimental and analytical techniques continue to generate much needed thermodynamic data constraining the solute loads of aqueous fluids in equilibrium with a variety of phase assemblages across a wide range of pressure and temperature. However, these techniques are constrained to systems with single-phase aqueous fluids. As alluded to above, detailed studies of natural aqueous fluids trapped as inclusions in a variety of host minerals (e.g., quartz, fluorite, topaz, anhydrite, olivine, clinopyroxene) indicate that evolving igneous and metamorphic systems are commonly saturated with coexisting aqueous vapor + brine owing to the wide miscibility gap in salt-water systems at *P-T* conditions applicable to much of Earth's lithosphere (Sourirajan and Kennedy 1962; Roedder 1984; Bodnar et al. 1985; Chou 1987a; Chou et al. 1992; Sterner et al. 1992; Anderko and Pitzer 1993; Heinrich et al. 1999; Manning 2004). If CO_2 is present, this miscibility gap may be even larger. Therefore, multi-phase fluid systems may be the rule rather than the exception. In light of the widespread recognition and apparent importance of immiscible aqueous fluids in the redistribution of elements in magmatic-hydrothermal ore-forming (and other igneous and metamorphic) environments, from traditional Cu-, Mo-, Au-rich porphyry-skarn deposits to Pt-group-element enriched zones within ultramafic layered intrusions, there is a need for an experimental technique that facilitates the in situ trapping of equilibrated, immiscible aqueous fluids at experimental *PTX* conditions directly applicable to the genesis of these various ore deposit types. Coupling such a technique with micro-analytical tools that quantify the solute loads of synthetic fluid inclusions provides the only means to constrain quantitatively the thermodynamics of element partitioning among coexisting multiphase fluids (i.e., silicate melt, sulfide melt, vapor, brine).

As a first step toward quantifying fully the thermodynamics of ore-metal-partitioning among coexisting vapor, brine, and silicate melt, over a wide range of *PTX* conditions relevant to element redistribution in ore-forming environments, we build upon the method of trapping synthetic fluid inclusions in pre-fractured quartz developed by Bodnar and Sterner (1985, 1987) and Bodnar et al. (1985). A major question surrounding synthetic fluid inclusion solute data is whether or not the coexisting volatile phases trapped as synthetic fluid inclusions had fully equilibrated with all system components at the *PTX* conditions of the run prior to entrapment (Simon et al. 2003a). We hypothesize that the data obtained from this method represent equilibrium conditions with all system components, specifically minor and trace elements, at the *PTX* conditions of the run prior to aqueous fluid entrapment. To test this hypothesis, we performed two separate experimental studies wherein aqueous, saline fluids (Au-saturated NaCl-KCl-HCl-$AuCl_2H$-H_2O±$FeCl_2$) were trapped at run *PTX* conditions as synthetic fluid inclusions, in (1) quenched melt (brine) and (2) pre-fractured quartz cores (co-existing vapor and brine). The data provide quantitative evidence that co-existing vapor and brine can be trapped in self-healed quartz fractures at *PTX* conditions after chemical equilibrium has been established throughout the charge.

Experimental procedures

Setup one: Brine vesicles

The first series of experiments was performed in a brine-haplogranite melt-Au metal capsule assemblage at 800 °C and 100 MPa (see Fig. 1). The purpose of these experiments was to provide Au concentrations in brine that was in equilibrium with Au-saturated melt. The data from this single-phase aqueous fluid will be compared with data from the two-phase fluid system (see below) to demonstrate that brines in the two-phase experiments contain equilibrium Au concentrations. On the order of 50 mg of synthetic haplogranite ($Qtz_{38}Ab_{33}Or_{29}$ on an anhydrous basis) and 80 mg of brine (NaCl + KCl + HCl) starting materials were loaded into an Au capsule

(4.8 mm ID, 5 mm OD, 30 mm length; the source of Au in all experiments). The haplogranite composition (Table 1) corresponds to the 100 MPa minimum melt composition and has a solidus temperature of ~710 °C. The bulk salinity of the brine (initial composition ~70 wt% NaCl eq.; initial K:Na = 0.5 to 1 and K/H = 3.2 to 104) was prepared so that the total chloride concentration corresponded to the brine-only phase stability field in the model NaCl-H_2O system at 100 MPa and 800 °C (Fig. 2; Sourirajan and Kennedy 1962; Bodnar et al. 1985; Chou 1987a; Chou et al. 1992; Sterner et al. 1992; Anderko and Pitzer 1993).

The porosity of the glass powder was controlled by varying the initial mechanical compression of the starting glass. A tightly packed starting glass results in very few trapped vesicles upon quench whereas a loosely packed starting glass yields a final glass with abundant trapped fluid in inclusions. Systematic variation of the initial porosity allowed us to control, and quantify, the volume of brine entering the melt and trapped, upon quench, as glass-hosted fluid inclusions at run *PTX* conditions. Loaded capsules were immersed in dry ice and welded shut. Sealed capsules were placed in a drying oven (110 °C) for 4 hours, and maintenance of capsule mass (±0.3 mg) was used to verify the mechanical integrity of welded capsules.

Setup two: Pre-fractured quartz

The second series of experiments employed pre-fractured quartz cores to trap coexisting vapor and brine as synthetic fluid inclusions at 800 °C and 110 MPa. Cores of natural quartz (Minas Gerais, Brazil) were cut to dimensions of approximately 1.5 cm long by 2 to 3 mm wide. The quartz cores were heated at 350 °C for 30 minutes and then fractured thermally by immersing them in a beaker of doubly deionized, distilled water. The temperature at which the cores were heated is based on Sterner and Bodnar (1984) and Bodnar and Sterner (1985, 1987). After recovering the cores from the water bath, the cores were dried at 120 °C for 4 hours to remove adsorbed water. Petrographic examination of quartz cores after this stage revealed a pervasive fracture network.

TABLE 1. Composition of synthetic haplogranite melt

Oxide	Wt%
SiO_2	75.18
Al_2O_3	11.09
K_2O	4.43
Na_2O	3.67
CaO	0.17
Fe_2O_3	0.04
MnO	0.01
MgO	0.10
TiO_2	0.03
P_2O_5	0.03
LOI	4.51
Total	99.26

Notes: Chemical composition of the starting glass used in all experiments as determined by XRF (Frank 2001). LOI = loss on ignition.

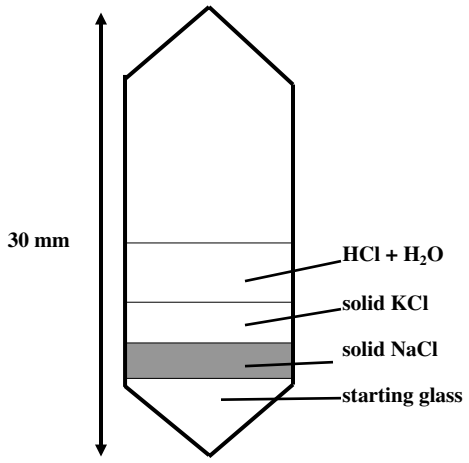

FIGURE 1. Schematic representation of experimental setup one used in this study. At run *P-T* conditions, the salts (NaCl, KCl, and HCl) and H_2O form a single-phase hypersaline liquid (i.e., brine).

A single, pre-fractured quartz core was loaded into a pure Au-metal capsule (dimensions identical to those reported above) along with approximately 40 mg synthetic haplogranite (composition given above), 40 mg magnetite (Cornwall, Pennsylvania), and 100 µL aqueous solution containing dissolved salts of NaCl, KCl, and HCl. Capsule dimensions were identical to setup 1. The capsule volume was set so that vapor occupied all open space inside the capsule and was in intimate contact with the melt, brine, and Au-metal capsule at run *P-T* conditions. Capsules were loaded and sealed as described above. A schematic depiction of the charge is provided in Figure 3. Magnetite was added to quantify magnetite solubility in aqueous vapor and brine; these data were reported elsewhere (Simon et al. 2004). The molar ratio of Na:K:H was set to unity in all starting aqueous solutions. The initial bulk salinity of aqueous fluid in the 110 MPa runs was 2.5 wt% NaCl eq. This bulk salinity lies just inside the vapor limb of the vapor-brine solvus in the model NaCl-H_2O system (Fig. 2); thus, the runs should be saturated with vapor and brine. Additional data from runs at 130, 140, and 145 MPa are included in this paper to highlight the effectiveness of using pre-fractured quartz cores to trap immiscible, saline fluids at run *PTX* conditions. The runs at 130, 140, and 145 MPa were vapor + brine saturated with bulk salinities of 5.5, 10, and 20 wt% NaCl eq., respectively.

Experimental conditions

The information here pertains to both experimental setups. The Au capsules were placed inside cold-seal René-41 pressure vessels and the system was pressurized using water as the pressure medium. Charges were pressurized at ambient temperature to approximately 50 MPa, heated to 800 °C and then pressurized to the final run pressure; thermal expansion of the water buffer acts to drive the charge toward the final pressure as the vessel is heated. Pressure was imposed by an air-driven water-pressure intensifier and monitored with Bourdon-tube gauges (±2 MPa) calibrated against a factory calibrated Heise gauge. Temperatures were measured with type K (Chromel-Alumel) external thermocouples. The temperature gradient in each experimental vessel was minimized by maintaining the hot end of the vessel and the furnace at a positive 10–12° angle from horizontal (following Charles and Vidale 1982). The center of the charge corresponds to the hotspot inside the vessel. The maximum temperature uncertainty at all pressures was ±5 °C over the 3 cm long capsule, as determined by internal calibration. This small

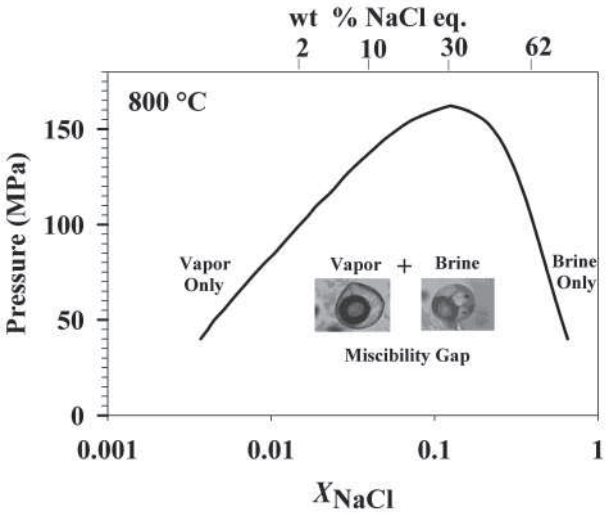

FIGURE 2. Isothermal section of the system NaCl-H_2O at 800 °C (modeled after Anderko and Pitzer 1993). X_{NaCl} = mole fraction of NaCl in the pure NaCl-H_2O system. The curve outlines the miscibility gap as a function of pressure at 800 °C; within this gap vapor and brine coexist as two immiscible and physicochemically distinct fluids. The inset photomicrographs (from Simon et al. 2004) of vapor (hypersaline fluid + vapor bubble at ambient conditions) and brine (hypersaline fluid + vapor bubble + halite ± other daughter crystals at ambient conditions) are from an experimental run product at 140 MPa. Salinity, expressed in units of wt% NaCl eq., values are presented along the upper abscissa; note that neither abscissa is a linear scale.

temperature gradient minimizes chemical potential gradients, which, in turn, eliminates the possibility of hot-end dissolution and cold-end precipitation of quartz in the charge. A small amount of water used as the pressure medium dissociates thermally at the *P-T* conditions of each run and the free oxygen, which reacts with the Ni-metal of the vessel (approximately 53 wt% Ni) to establish an intrinsic hydrogen fugacity buffered at Ni-NiO (NNO; Chou 1987b). The diffusion of hydrogen from the water-pressure medium through the Au-capsule walls into the charge and subsequent osmotic equilibration of hydrogen buffers the charge assemblage at NNO. At 800 °C, the experimental vessels used in this study have oxygen fugacities of $\log f_{O_2} = -14.0 \pm 0.1$ as determined in our laboratory using the Ag-AgCl sensor technique (Chou 1987b). Experiments were quenched isobarically along a two-stage cooling path involving air-stream cooling from 800 to 200 °C followed by immersion in an ambient-temperature water bath. Capsules were removed from the vessels, cleaned, examined microscopically, and weighed to determine if the capsules remained sealed during the experiment. Only capsules that exhibited mechanical integrity were processed for analysis.

Characerization of run products

Glass recovered from experiments of setup 1 contained brine fluid inclusions and the proportion of brine inclusions varied directly with the initial porosity of the starting glass powder (i.e., low initial porosity yielded few trapped inclusions whereas high initial porosity yielded glass with a significant number of fluid inclusions). Petrographic analysis of run-product glasses verified that the runs were vapor-undersaturated. The glasses were optically homogeneous and contained no visible solid phases. Brine inclusions contained one or more salt crystals (i.e., halite and sylvite), a vapor bubble, and liquid. Phase proportions were constant for all brines in all experiments. No attempt was made to recover the non-glass components of the charge. These phases consisted of aqueous fluid and precipitated salts.

Quartz cores recovered from experiments of setup 2 contain *both vapor and brine fluid inclusions* trapped in healed microfractures. Silicate glass from these runs was optically homogeneous and lacked visible solid phases. Optical examination of all surfaces of the recovered quartz core indicated that no new overgrowths formed. No melt inclusions were observed in healed fractures; however, these were not the focus of the current study and, thus, no significant time was invested in searching for them. A photomicrograph of coexisting vapor plus brine is provided in Figure 4. Vapor inclusions contain liquid plus a vapor bubble whereas brine inclusions contain liquid, a vapor bubble, and halite ± additional daughter mineral phases. At least one salt crystal was visible in all brine inclusions. Magnetite, inferred from crystal morphology and its response to a strong magnet, was visible in larger brine inclusions and inferred to be present in all brine inclusions. Vapor and brine were trapped together (i.e., boiling assemblage) and separately in healed microfractures. Inclusions range in size from <5 to 30 µm with the majority of inclusions being <20 µm. The phase proportions of vapor and brine inclusions are nearly constant for fluid inclusion populations in quartz cores. Some "vapor" inclusions contained a higher proportion of liquid to vapor that most likely reflects the accidental entrapment of a small quantity of brine. These inclusions were noted and eliminated from further study. Details on the salinities, final ice melting, and homogenization temperatures, etc. are provided below. The quenched aqueous solutions in runs from setup two were removed by hypodermic syringe and processed as discussed below.

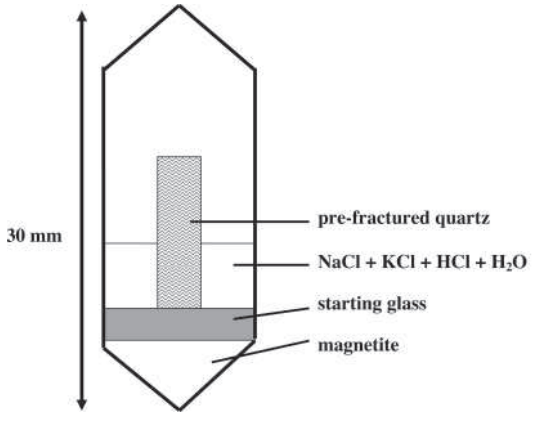

Figure 3. Schematic representation of experimental setup two used in this study. At run *P-T* conditions, the starting NaCl + KCl + HCl aqueous fluid separates into co-existing low-salinity vapor and high-salinity brine.

Analytical procedures

Analyses of experimental glasses

A JEOL JXA 8900 electron microprobe equipped with five wavelength-dispersive spectrometers (WDS) was used to characterize quantitatively the major-element and Cl concentrations of run-product silicate glasses; analyses done at the Center for Microanalysis, University of Maryland. Glass samples were mounted, polished, and coated with a ~0.03 µm carbon film. Operating conditions for glass analyses were 15 keV accelerating potential, 5 nA beam current, and a 15 µm beam size with a minimum counting time of 20 seconds (sum of peak and background). Multiple line traverses were performed on each glass to evaluate melt homogeneity for both major and minor elements. Numerous analyses were performed to evaluate the effects of Na diffusion and Si and Al burn-in (Morgan and London

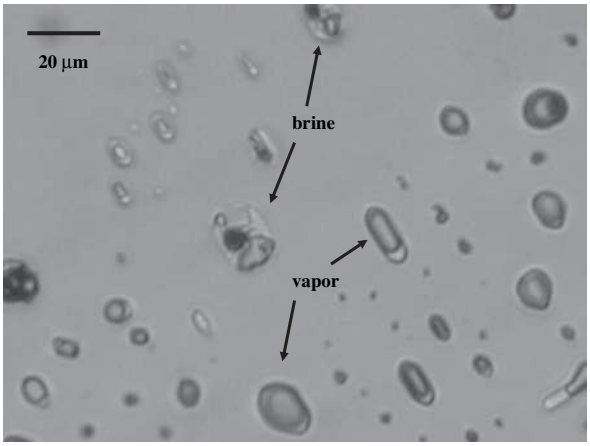

Figure 4. A representative photomicrograph of coexisting vapor plus brine fluid inclusions trapped in quartz at 110 MPa. The two vapor and two brine inclusions were trapped within a single, self-healed, fracture at run conditions (110 MPa and 800 °C). The brine inclusion contains a vapor bubble, liquid, and daughter crystals of halite, sylvite, and magnetite. The vapor inclusion contains a vapor bubble and liquid.

1996; Acosta-Vigil et al. 2003). No systematic Na migration was observed in glasses. Standardization for Si, Al, Na, and K was performed with a Yellowstone rhyolite (National Museum of Natural History, NMNH 72854 VG568). Kakanui hornblende was used to standardize Fe. Scapolite (Meionite, Brazil, USNM R6600-1) was used to standardize Cl.

The Au concentrations of silicate glass in experimental setup 1 were determined by secondary ion mass spectrometry (SIMS performed by Rick Hervig at ASU) using the negative secondary ions and a K primary beam (30 μm diameter) to bombard the sample (McMahon et al. 2000). A normal incidence electron gun was used to alleviate charge, and three NIST glass standards (610, 612, and 614) were used to calibrate the signal. A crater was sputtered on the sample glass, and the ion intensities for ^{18}O, ^{30}Si, ^{35}Cl, and ^{197}Au were collected. Chlorine was monitored to detect the presence of fluid inclusions in glass volumes; these analyses were rejected. The ion signals were integrated for 5 seconds during each cycle and the total number of cycles ranged from 30 to 82, translating to a total analysis time of 15 to 30 minutes. Counting statistics indicated that the relative error for each cycle was at least 20%. The integrated Au signal indicated a counting error ranging from 20% on the lowest Au sample to 2% on the highest Au sample.

The Au concentrations of silicate glass recovered from experiments of setup 2 were quantified by LA-ICPMS; analyses performed at ETH, Zurich. Spots optically devoid of fluid inclusions were analyzed with a 90 μm spot size. Samples were placed in a 1 cm^3 ablation chamber and an energy homogenized (Microlas), pulsed 193-nm ArF Excimer laser (Compex 110i, Lamda Physik) that enables controlled ablation (Günther et al. 1997, 1998; Heinrich et al. 2003) was used to ablate silicate glass directly into the ICPMS. Helium was used as the carrier gas to improve the aerosol uptake rate (Eggins et al. 1998; Günther and Heinrich 1999). The ICPMS instrument (ELAN quadrupole mass spectrometer) settings were similar to those reported in Pettke et al. (2004); dual detector mode was used and the isotope ^{197}Au was monitored with a dwell time of 30 ms. NIST-610 was used as the reference silicate glass standard and the Si concentration of the glass, determined by EPMA, was used as the internal standard to calculate absolute Au concentrations. NIST-610 is not a NIST certified Au standard; however, the NIST informative value of 25 μg/g agrees well with the globally accepted value of 22.5 ± 3.5 μg/g (1 standard deviation of the preferred average) as reported in Pearce et al. (1996). Thus, in agreement with many laboratories around the world, we suggest that NIST-610 can be used as an Au standard for the analysis of silicate glasses. LA-ICPMS analyses revealed the presence of Au nuggets in silicate glass from all experiments. Gold is notorious for precipitating from silicate melt as the melt cools through the glass transition temperature, as discussed in Frank et al. (2002). The source of the Au present in the glass as an Au nugget cannot be determined. As such, Au nuggets may have precipitated from the ablated glass volume and, thus, their removal artificially lowers the calculated Au concentration relative to the concentration of Au present in the ablated volume of glass prior to passing through the glass transition temperature. We suggest that removal of the Au particles during signal processing inherently biases the final data and, thus, all glass analyses were processed by integrating over the entire signal. In spite of the relatively high uncertainty that results, this method eliminates human-introduced bias into the data set (i.e., we did not massage the data) and yields a final average Au solubility that is consistent with data from other analytical techniques [i.e., Instrumental Neutron Activation Analysis (INAA), SIMS].

Analyses of brine vesicles from setup one

The concentration of Au in glass-hosted vesicles was quantified by bulk INAA; analyses done at the University of Missouri Research Reactor Center. All fragments of glass recovered from each experiment were soaked in aqua regia for at least 5 minutes to remove adsorbed Au. The glass fragments were then rinsed with doubly deionized and distilled water, allowed to soak in a water bath for at least 10 minutes, and rinsed an additional 10 minutes to ensure that all aqua regia was removed. We did not analyze any fragments without first leaching them. Three standards were placed along with the samples in high-density polyethylene vials and irradiated for 30 seconds with a neutron flux of 8×10^{13} n × cm^{-2} × s^{-1}. The concentration of ^{38}Cl (half-life of 37.2 minutes) was quantified using the 2168-keV gamma ray and a hyperpure germanium (HPGe) detector with a count time of 12 minutes; samples were placed 10 cm from the detector. Samples were then allowed to decay for 18 to 24 hours to reduce the concentration of short-lived nuclides. Counting for ^{198}Au was performed for 60 minutes at the 412-keV gamma ray. The samples and standards were rotated during counting to minimize analytical uncertainty (Glascock 1998). The concentration of Au in the brine + glass mixture was regressed against the mass fraction of brine in the mixture, as discussed in Frank et al. (2002).

The absolute concentration of Au in brine inclusions was determined by mass balance. Varying the porosity of the silicate melt yielded experimental glasses with mass fractions of brine (mf_b) that ranged from 2.9 to 4.9 %. The mass fraction of brine was determined by mass difference of the initial glass added to each capsule and the final mass of the glass bead recovered from the experiment taking into consideration the water solubility of the melt. These values were calculated for each glass by relating the total chloride concentration of the brine and glass to the chloride analyses of the glass + brine mixtures. Note that the chloride concentration of brine was kept constant by using a high mass ratio of brine to melt in all experiments. The concentration of Au in the brine + glass mixture (C_{Au}^{b+g}) is related to the concentration of Au (C_{Au}^{b}) in the brine by the equation:

$$C_{Au}^{b} = \left[\frac{C_{Au}^{b+g} - (C_{Au}^{g} \times mf_g)}{mf_b} \right] \quad (1)$$

where mf_b is the mass fraction of brine in the brine + glass mixture, mf_g is the mass fraction of glass in the brine + glass mixture, and C_{Au}^{g} is the concentration of Au in the glass. The HCl concentrations of brine were calculated from the mass transfer of alkalis between the melt and brine by using the starting compositions and masses of the melt and brine and the final composition of the melt. Interested readers are referred to Frank et al. (2002) for further details.

Analyses of synthetic fluid inclusions from setup two

Microthermometry. Recovered quartz cores were set in Crystalbond 509 Mounting Adhesive, sectioned longitudinally into wafers (~500 µm thick), and then polished on both sides for petrographic examination, microthermometry, and LA-ICPMS analysis. Salinities of vapor and brine inclusions were determined by freezing point depression (i.e., Tm_{ice}) and final dissolution of halite (i.e., Td_{NaCl}), respectively, using a USGS-type gas flow heating-freezing stage (Fluid, Inc.). The heating-freezing stage was calibrated at –56.6 °C (the melting temperature of pure CO_2), 0 °C (the melting temperature of pure H_2O), and 374.1 °C (the critical temperature of pure H_2O). Uncertainties in final ice melting and homogenization temperatures are ±0.2 and ±1.2 °C, respectively. The thermocouple was placed directly on the sample to hold the sample and reduce uncertainty in temperature measurements. All analyzed fluid inclusions displayed consistent phase ratios. Although we analyzed only a limited number of vapor and brine inclusions, the phase ratios in these inclusions are consistent with those in the remainder of non-analyzed fluid-inclusion population in each quartz core. Additionally, the inclusions chosen for analysis come from different parts of the quartz core (i.e., are trapped in multiple healed fractures). We feel that the fluid-inclusion-selection methodology is statistically robust and provides a high-quality assessment of fluid inclusions trapped throughout the quartz core.

Apparent salinities for magmatic vapors and brines were calculated using the equations of Bodnar and Vityk (1994). Ice-melting temperatures, homogenization temperatures, and apparent salinities for the 110 MPa experiments are reported for vapors and brines in Table 2. The data for vapor and brine fluid inclusions trapped at 130, 140, and 145 MPa are reported in Tables 3–5. The reported salinities in this study agree with those expected for the NaCl-KCl-$FeCl_2$-HCl-H_2O system based on extant data for the model systems NaCl-H_2O and NaCl-KCl-H_2O (Sourirajan and Kennedy 1962; Bodnar et al. 1985; Chou 1987a; Chou et al. 1992; Sterner et al. 1992; Anderko and Pitzer 1993). The agreement between the new and extant data sets suggests that the addition of $FeCl_2$ and HCl, in proportions analogous to natural magmatic-hydrothermal aqueous fluids, does not alter significantly the location of the solvus in the NaCl-KCl-H_2O system.

LA-ICPMS analyses. The solute concentrations of synthetic vapor and brine inclusions were quantified individually by LA-ICPMS using an energy-homogenized (Microlas), pulsed 193 nm ArF Excimer laser as described above. The diameter of the laser beam was set slightly larger than the maximum dimension of each fluid inclusion to ensure that the entire inclusion was ablated together with a minimal volume of surrounding matrix quartz. The number of fluid inclusion analyses reported here may differ from the total number of inclusions for which microthermometry data are reported. This results from the inability to analyze some inclusions, owing to depth issues, and/or the loss of solutes from some inclusions when ablated very close to the surface.

A representative LA-ICPMS transient signal of a vapor inclusion ablated from a depth of ca. 50 µm is shown in Figure 5. The signal consists of gas background (0–20 and 91–100 s), host quartz (21–67 and 80–91 s), and quartz plus vapor fluid inclusion (67–80 s). The transient signal for each analysis was integrated and element ratios (e.g., Au:Na) were quantified using a NIST SRM 610 silicate glass. The ability of silicate glass standards to quantify solute loads of fluid inclusions has been demonstrated by Günther et al. (1998) and interested readers are directed there for more information on the technique. Element ratios determined by LA-ICPMS were transformed into absolute element concentrations using Na as the internal standard. Absolute concentrations of Na in each fluid inclusion were determined by correcting the apparent salinity, wt% NaCl eq. determined by microthermometry, for the presence of other chloride salts via the equation,

$$NaCl_{true} = NaCl_{equivalent} - 0.5 \times \Sigma X^{n+}Cl_n \quad (2)$$

originally presented in Heinrich et al. (1992). This equation treats all major cations in fluid inclusions as chloride salts, an assumption that has been tested and verified by Heinrich et al. (1992, 2003). The equation is based on the similar solubility behavior for NaCl-KCl-H_2O (Roedder 1984; Sterner et al. 1992) and NaCl-$CaCl_2$-H_2O (Vanko et al. 1988) systems and NaCl-dominant aqueous fluids, as discussed at length in Heinrich et al. (1992, 2003). The calculated true Na concentrations for each fluid inclusion were then used to calculate the concentration of other metals in the fluid inclusion (flinc) following the methods outlined in Heinrich et al. (2003). It should be noted that the equation above was originally formulated in Heinrich et al. (1992) from data obtained at temperatures lower than those of the current study and in experimental systems lacking $FeCl_2$. Simon (2003) quantified the solubility of magnetite in high-temperature vapor and brine and concluded that the addition of $FeCl_2$ to the NaCl-KCl-HCl-H_2O system does not cause statistically meaningful changes to the solvus relative to the Fe-free system. These equations have been tested in previous studies and

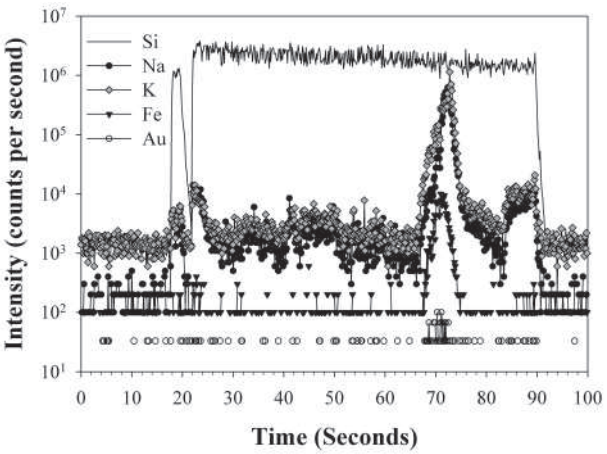

FIGURE 5. LA-ICPMS transient signal of a vapor-rich fluid inclusion (~20 µm across; ~50 µm deep; 2.1 wt% NaCl eq.) hosted within quartz. A 40 µm beam diameter was used to ablate the entire inclusion. Ablation of quartz began at ~20 seconds and the fluid inclusion was liberated from ~67 to 80 seconds. The first few seconds of the ablation signal contains surficial contaminants (Landtwing and Pettke 2005) that are flushed through the system prior to the ablation of the fluid inclusion. The signal between 85 and 90 seconds represents a second inclusion ablated incompletely from deeper in the quartz host. This signal is time resolved from the first inclusion (67 to 80 seconds) and, thus, contributes nothing to the reported concentration for the targeted fluid inclusion.

TABLE 2. Microthermometric data for vapor and brine fluid inclusions trapped in experimental setup two at 800 °C and 110 MPa

Vapor fluid inclusions	Final ice-melting temperature (°C)	Calculated wt% NaCl eq.	Brine fluid inclusions	Homogenization temperature (°C)	Calculated wt% NaCl eq.
	Run 60			Run 60	
1	–1.4	2.4	1	475	59.5
2	–1.2	2.1	2	468	58.4
3	–1.3	2.2	3	472	59.0
4	–1.3	2.2	4	465	57.9
5	–1.4	2.4	5	460	57.1
6	–1.4	2.4	6	471	58.9
			7	475	59.5
	Run 61			Run 61	
7	–1.4	2.4	8	469	58.5
8	–1.4	2.4	9	463	57.5
9	–1.2	2.1	10	467	58.2
10	–1.4	2.4	11	472	59.0
11	–1.2	2.1	12	461	57.2
12	–1.3	2.2		Run 62	
13	–1.2	2.1	13	460	57.1
14	–1.4	2.4	14	472	59.0
			15	463	57.5
	Run 62		16	475	59.5
15	–1.3	2.2	17	469	58.5
16	–1.4	2.4	18	468	58.4
17	–1.2	2.1	19	466	58.0
18	–1.2	2.1			

TABLE 3. Microthermometric data for vapor fluid inclusions trapped in experimental setup two at 800 °C and 130 MPa

Vapor fluid inclusions	Final ice-melting temperature (°C)	Calculated wt% NaCl eq.	Brine fluid inclusions	Homegenization temperature (°C)	Calculated wt% NaCl eq.
	Run 40			Run 40	
1	–3.1	5.1	1	431	52.7
2	–3.2	5.3	2	424	51.7
3	–2.9	4.8	3	417	50.8
4	–3.0	5.0	4	409	49.7
5	–3.1	5.1	5	426	52.0
	Run 52			Run 52	
6	–3.2	5.3	6	418	50.9
7	–2.9	4.8	7	431	52.7
8	–3.1	5.1	8	415	50.5
9	–3.0	5.0	9	429	52.4
10	–3.2	5.3	10	425	51.8
			11	430	52.6
	Run 55				
11	–3.1	5.5		Run 55	
12	–3.1	5.1	12	421	51.3
13	–3.3	5.4	13	416	50.6
14	–2.9	4.8	14	429	52.4
15	–3.0	5.0	15	430	52.6
16	–2.8	4.6	16	422	51.4
17	–3.1	5.1	17	418	50.9
18	–3.3	5.4	18	424	51.7
			19	491	62.3
			20	433	53.0
			21	414	50.4

found to yield accurate element concentrations in fluid inclusions trapped at high temperatures (Günther et al. 1997, 1998). Furthermore, the equations have been used to generate data that have been accepted and published in numerous studies of high-temperature fluid inclusions (Audétat et al. 1998, 2000; Ulrich et al. 1999, 2001; Halter et al. 2002; Audétat and Pettke 2003; Redmond et al. 2004; Hanley et al. 2005; Landtwing and Pettke 2005; Landtwing et al. 2005; Simon et al. 2005). The comparison of LA-ICPMS, INAA, and AAS data presented and discussed below demonstrate that Equation 2 is valid for temperatures to at least 800 °C. Interested readers are referred to Heinrich et al. (2003) for further discussion.

Analyses of quenched fluids from experiment setup two

Recovered capsules were placed in dry ice to cool the quenched aqueous fluid. Cooling the capsule prevents loss of aqueous fluid owing to overpressure inside the capsule. After several minutes of cooling, the top end of the capsule (i.e., end of capsule elevated furthest from the horizontal plane on which the experimental apparatus assembly rests) was pierced with a stainless steel hypodermic syringe. Blanks were prepared and analyzed by sampling prepared acidic solutions with the syringes. These trials indicated convincingly that the no Fe was leached from the syringe by the recovered solutions during transfer. Recovered aqueous solutions were weighed and diluted for analysis by AAS; analyses performed in the Department of Geology, University of Maryland. An air-acetylene flame was used to quantify the concentrations of Na, K, and Fe. Concentrations were determined by linear regression using a six-point standard calibration curve within the linear working range for the analytical instrument as verified for each element in our laboratory.

The HCl concentration of the quenched experimental fluids

TABLE 4. Microthermometric data for vapor and brine fluid inclusions trapped in experimental setup two at 800 °C and 140 MPa

Vapor fluid inclusions	Final ice-melting temperature (°C)	Calculated wt% NaCl eq.	Brine fluid inclusions	Homogenization temperature (°C)	Calculated wt% NaCl eq.
	Run 47			Run 47	
1	–5.9	9.1	1	347	42.6
2	–6.2	9.5	2	350	42.9
3	–5.9	9.1	3	359	43.8
4	–6.1	9.3	4	362	44.1
5	–6.2	9.5	5	355	43.4
			6	344	42.3
	Run 49		7	353	43.2
6	–6.1	9.3			
7	–5.7	8.8		Run 49	
8	–5.9	9.1	8	361	44.0
9	–6.2	9.5	9	343	42.2
10	–6.1	9.3	10	355	43.4
11	–5.8	8.9	11	359	43.8
12	–6.0	9.2	12	356	43.5
13	–5.8	8.9	13	348	42.7
14	–5.9	9.1	14	357	43.6
15	–5.7	8.8	15	342	42.1
16	–6.1	9.3	16	345	42.4
17	–5.9	9.1	17	358	43.7
18	–6.0	9.2			
19	–5.9	9.1			

TABLE 5. Microthermometric data for vapor and brine fluid inclusions trapped in experimental setup two at 800 °C and 145 MPa

Vapor fluid inclusion	Final ice-melting temperature (°C)	Calculated wt% NaCl eq.	Brine fluid inclusion	Homogenization temperature (°C)	Calculated wt% NaCl eq.
	Run 59			Run 59	
1	–15.0	18.6	1	274	36.4
2	–15.9	19.4	2	263	35.6
3	–15.6	19.1	3	265	35.7
4	–15.3	18.9	4	275	36.4
5	–16.0	19.4	5	284	37.1
6	–15.8	19.3	6	260	35.4
7	–15.4	19.0	7	277	36.6
8	–15.1	18.7	8	269	36.0
		9	258	35.3	
	Run 63		10	262	35.5
9	–15.0	18.6			
10	–15.7	19.2		Run 63	
11	–15.2	18.8	11	281	36.9
12	–16.0	19.4	12	276	36.5
13	–15.1	18.7	13	272	36.2
14	–15.3	18.9	14	265	35.7
15	–15.6	19.1	15	253	34.9
16	–15.4	19.0	16	268	36.0
17	–15.3	18.9	17	274	36.4
18	–15.6	19.1	18	263	35.6
		19	281	35.3	

was determined measuring fluid pH by using a Beckman φ40 pH meter equipped with an AccupHast electrode. In order to quantify properly the activity vs. concentration function for hydrogen ion in the quenched solutions, we prepared pH standards with reagent grade HCl to define a pH range that overlapped the expected pH of the quenched solutions and we added reagent-grade NaCl and KCl in proportions corresponding to the expected concentrations of these salts in the quenched experimental solutions. This procedure minimizes the error owing to matrix effects on the measured pH values. The determined M_{H+} in the quenched fluid is assumed to represent the hydrogen ion concentration that was present as associated HCl in the experimental fluid as HCl completely dissociates during quench (Tagirov et al. 1997). Whereas this assumption ignores the possibility of sub-solidus reactions that can affect the M_{H+}, all charges were analyzed within one to two hours of quench and, thus, we feel that this assumption is justified. It should be noted that the potentiometrically determined hydrogen concentrations represent the hydrogen in the quenched aqueous fluid, consisting of coexisting vapor and brine at run conditions. The proportion of vapor: brine in the quenched aqueous mixture is >95:1. Owing to the strong partitioning of HCl into vapor coexisting with brine (Williams et al. 1997), we infer the measured HCl concentrations to approximate the HCl concentration of the experimental vapor.

RESULTS

Glass compositions

The major element, Cl, and Au contents of glass reported in Table 6 indicate that the melts are chemically homogeneous. The final glass composition indicates that components were exchanged between the aqueous fluid and melt. The aluminum saturation index (ASI) of the starting glass was 1.01. A decrease in the ASI indicates that the melt has gained Na and K from the saline aqueous fluid. This is consistent with the low HCl concentrations of the experiments, which should yield peralkaline

melts (Candela 1990). The glass data, coupled with the microthermometry data for aqueous fluid (discussed below), suggest that chemical equilibrium between melt and aqueous fluid was achieved prior to quench. The average Au concentration of all glasses recovered from experiment setup 1 is 0.9 ± 0.4 μg/g. This datum agrees with the Au concentration determined by INAA for silicate glasses with mass fractions of brine less than 5%. SIMS analyses revealed the presence of Au "nuggets" in portions of silicate glass. These nuggets are interpreted to form during quench as the Au solubility of the silicate melt drops and micro-particles of Au precipitate from the melt and are trapped in glass. The SIMS data reported here were determined by integrating the SIMS signal over time. The result of all glass analyses from experiment setup 2 indicate that Au concentrations in silicate melts in equilibrium with aqueous vapor and brine range from 0.25 to 1 μg/g at pressures from 110 MPa to 145 MPa. The average value of 0.8 ± 0.3 μg/g for experiments at 110 MPa is consistent with the value of 0.9 ± 0.4 μg/g reported above. Slightly lower mean values for Au solubility of 0.6 ± 0.3, 0.5 ± 0.2, and 0.5 ± 0.2 μg/g were determined at 130, 140, and 145 MPa, respectively. The implications of these Au solubility data for the evolution of silicate melts are discussed at length in Frank et al. (2002; experiment setup 1) and in Simon et al. (2003b, 2005; experiment setup 2), respectively.

Gold concentrations in glass- and quartz-hosted inclusions

The glass-hosted brine inclusions were trapped as the melt passed through the glass transition upon quench. Thus, these brine inclusions preserve fluid compositions in equilibrium with the melt and Au capsule until the moment of run termination. Microthermometry data for quartz-hosted brines indicate that their salinities agree with the model NaCl-KCl-H_2O system. The salinity of vapor and brine are on the order of 2–4 and 58–60 wt% NaCl eq., respectively, in the NaCl-KCl-H_2O system. The agreement between actual and predicted salinities evinces that the quartz-hosted brine inclusions were trapped at run *P-T* conditions prior to quench, albeit the exact time of entrapment cannot be quantified. However, the statistically overlapping Au concentrations in the glass- and quartz-hosted brine inclusions suggest that the quartz-hosted brine inclusions were trapped after the brine reached equilibrium with respect to Au metal (Table 7). One further point to consider is that the brine co-existed with vapor in the quartz-bearing experiments. However, the presence of vapor should not cause a change in the final Au solubility of brine. The only difference between the brine-only and vapor + brine experiments lies in the final salinity of brine at 100 and 110 MPa. The final salinity of the brine decreases from 61–63 to 57–59 wt% NaCl eq. as pressure increases from 100 to 110 MPa, respectively. However, the Au-carrying potential of brine is not strictly dependent on total salinity. Rather, the concentration of Au, present most likely as $AuCl_2H$ in the brine (Frank et al. 2002), is thought to be controlled by the HCl concentration in the brine (Frank et al. 2002; Stefánsson and Seward 2003; Simon et al. 2005). Thus, the Au concentrations should be similar if the HCl concentrations of both glass-hosted and quartz-hosted brine are similar. We cannot determine directly the HCl concentration of the quartz-hosted brine. However, we can infer that the HCl concentrations of both glass-hosted and quartz-hosted brine are similar. The HCl concentration of the brine plays a role in controlling the HCl concentration of the melt that in turn plays a role in controlling the ASI of the melt. Peralkaline melts are expected to yield magmatic volatile phases with lower HCl concentrations relative to higher-aluminosity melts (Candela 1990; Candela and Piccoli 1995; Williams et al. 1997). The ASI values reported for glasses from experimental setups one and two indicate that all glasses are mildly peralkaline (Table 6). We suggest that the similar bulk salinity of all brine, both quartz- and glass-hosted, and the slightly peralkaline nature of all glasses, indicate that the HCl concentration of brines in both studies are similar. Thus, if the HCl concentration of brine controls Au solubility in the brine (Frank et al. 2002), the Au concentrations of all brines should overlap.

The Au concentrations of glass- and quartz-hosted brine fluid inclusions are presented in Table 7. These quartz-hosted inclusions were trapped in the 110 MPa experiments. Au concentrations (±2σ) in quartz-hosted fluid inclusions and glass-hosted

TABLE 6. EPMA analyses of major elements and chlorine in the run product glasses

Run No.	Pressure (MPa)	SiO_2 wt% (±2σ)	K_2O wt% (±2σ)	Na_2O wt% (±2σ)	FeO wt% (±2σ)	Al_2O_3 wt% (±2σ)	Cl wt% (±2σ)	Au (μg/g)	Total	ASI*
Glass from setup one										
5	100	75.00 ± 0.66	6.42 ± 0.28	2.79 ± 0.24	BD†	11.04 ± 0.50	0.20 ± 0.02	0.9 ± 0.4	95.45	0.96
8	100	75.26 ± 0.8	6.17 ± 0.20	2.88 ± 0.38	BD†	10.80 ± 0.30	0.17 ± 0.02	0.9 ± 0.4	95.28	0.95
9	100	75.74 ± 0.34	6.10 ± 0.12	2.46 ± 0.16	BD†	10.75 ± 0.28	0.18 ± 0.04	0.9 ± 0.4	94.23	1.00
10	100	77.1 ± 0.18	4.94 ± 0.48	3.44 ± 0.62	BD†	10.70 ± 1.60	0.07 ± 0.02	0.9 ± 0.4	96.25	0.97
Glass from setup two										
60	110	72.11 ±1.55	5.10 ± 0.42	4.87 ± 0.38	1.45 ± 0.46	11.61 ± 0.85	0.21 ± 0.08	0.73 ± 0.3	93.97	0.86
61	110	73.28 ± 1.86	4.80 ± 0.33	3.70 ± 0.31	1.16 ± 0.29	10.88 ± 0.75	0.18 ± 0.05	0.75 ± 0.3	95.32	0.97
62	110	73.85 ± 1.95	4.75 ± 0.28	4.43 ± 0.42	1.7 ± 0.35	10.29 ± 0.64	0.2 ± 0.07	0.92 ± 0.3	95.23	0.83
40	130	72.74 ± 1.40	5.30 ± 0.32	4.14 ± 0.29	0.91 ± 0.17	10.64 ± 0.81	0.23 ± 0.03	0.55 ± 0.3	93.96	0.85
52	130	73.24 ± 0.95	5.11 ± 0.19	4.28 ± 0.17	1.14 ± 0.24	10.81 ± 0.71	0.18 ± 0.05	0.63 ± 0.3	94.76	0.86
55	130	71.98 ± 1.22	5.22 ± 0.25	4.49 ± 0.28	1.22 ± 0.39	11.31 ± 0.93	0.2 ± 0.04	0.58 ± 0.3	94.42	0.87
47	140	74.35 ± 1.13	5.06 ± 0.34	3.55 ± 0.36	1.01 ± 0.24	10.01 ± 0.71	0.19 ± 0.06	0.52 ± 0.2	94.33	0.89
49	140	72.65 ± 0.74	5.28 ± 0.24	4.01 ± 0.26	1.05 ± 0.34	10.84 ± 0.58	0.23 ± 0.04	0.47 ± 0.3	94.10	0.88
59	145	72.84 ± 0.85	4.95 ± 0.23	3.14 ± 0.19	1.09 ± 0.41	9.21 ± 0.68	0.19 ± 0.06	0.45 ± 0.3	91.42	0.87
63	145	72.59 ± 1.30	5.48 ± 0.17	3.55 ± 0.34	1.05 ± 0.22	10.35 ± 0.66	0.22 ± 0.05	0.53 ± 0.3	93.24	0.88

Notes: Gold concentrations were determined by LA-ICPMS. Each datum represents the average of a minimum of ten spot analyses in different areas of a given experimental glass. Uncertainties are presented as twice the standard deviation from the mean (±2σ) for the replicate measurements of each glass. Data for runs 5, 8, 9, and 10 originally presented in Frank et al. (2002). Data from all other runs from Simon et al. (2005).

* ASI was calculated as the molar ratio [$Al_2O_3/(Na_2O + K_2O)$]. The calculated values of ASI indicate that all experimental melts were peralkaline.

† FeO was not added to these runs, but was included in the analytical menu.

vesicles are 29 ± 4 and 38 ± 17 μg/g, respectively. The larger uncertainty in the glass-hosted brine inclusion is a function of one experiment that yielded an Au concentration of 63 μg/g relative to the range of 25 to 39 μg/g for the other four runs. Dixon's Q-test was used to address this inconsistent datum. The Q (observed) is equivalent to a risk of false rejection of 5% at the Q_{10} statistical level. Hence, the higher datum is inconsistent with the data set and was removed; this yields a mean Au content in the INAA-quantified brine of 30 ± 8 μg/g, statistically identical to the value of 29 ± 4 for the quartz-hosted brines. The pressure difference of 10 MPa, and corresponding slight increase in brine salinity, between experimental setups one and two exerts no statistically discernible effect on the Au content of the brines. The overlap in Au contents of the quartz-hosted and glass-hosted brines suggest that the brines trapped in healed quartz microfractures reached equilibrium with respect to Au metal prior to entrapment.

Na, K, and Fe concentrations in quenched aqueous fluid and quartz-hosted vapor inclusions

The mass ratio of vapor to brine in all experiments from setup 2 is >95:1, determined using the lever rule and the salinities of the initial aqueous solution and measured wt% NaCl eq. values for the vapor and brine fluid inclusions. The high salinity of the brine relative to the vapor indicates that even at low mass fractions, the brine may contribute to the solute load of the quenched aqueous solution (i.e., rehomogenized vapor and brine). However, data from the current study suggest that rehomogenization during quench imparts a minimal additive chemical effect to the quantified solute loads of quenched aqueous mixtures at pressures ≤110 MPa.

The concentrations of Na, K, and Fe in synthetic fluid inclusions and the major-element solute load of recovered, quenched aqueous fluid from setup two are provided in Table 8. The presence of Fe in the quenched aqueous fluids and trapped fluid inclusions demonstrates that the starting fluids reacted with magnetite at run *P-T* conditions. Sodium concentrations (±2σ) in quenched aqueous fluid and vapor fluid inclusions are 6400 ± 520 and 5500 ± 840 μg/g, respectively. Potassium concentrations (±2σ) in quenched aqueous fluid and vapor fluid inclusions are 6000 ± 780 and 5800 ± 800 μg/g, respectively. Iron concentrations (±2σ) in quenched aqueous fluid and vapor fluid inclusions are 3100 ± 350 and 3100 ± 740 μg/g, respectively. The concentrations of Na, K, and Fe are invariant with respect to time. These statistically overlapping time-invariant and time-invariant major-element concentrations evince that fluid inclusions chosen for LA-ICPMS analysis contained fully equilibrated solute loads with respect to the metals Na, K, and Fe. We highlight that the 2σ overlap in the Na, K, and Fe concentrations further validate the use of equations described above to calculate metal concentrations in multi-component saline fluid inclusions as discussed in Heinrich et al. (1992, 2003).

TABLE 7. Gold and HCl concentrations in glass-hosted (100 MPa) and quartz-hosted (110 MPa) brine inclusions trapped in experimental setups one and two

Run no.	Au (μg/g)	HCl (μg/g)
Glass hosted brines*		
5	63 ± 2.5	900 ± 500
8	25 ± 2	900 ± 300
9	40 ± 2	1000 ± 400
10	25 ± 2	300 ± 100
Quartz-hosted brines†		
60	32 ± 9	ND‡
61	21 ± 11	ND‡
62	38 ± 7	ND‡

* These data originally published in Frank et al. (2002).
† These data originally published in Simon et al. (2005).
‡ The HCl concentrations of brines in setup 2 were not quantitatively determined, as discussed in the paper.

Experiments at higher pressure

Experimental data from runs at pressures greater than 110 MPa suggest that salts of Na, K, and Fe precipitate from aqueous fluid during quench. No attempt was made to recover precipitated solids from the capsule. Rather, the concentrations of Na, K, and Fe in quenched aqueous fluids (AAS) and quartz-hosted vapor-fluid inclusions (LA-ICPMS) from experiments at 130, 140, and 145 MPa were compared to evaluate the loss of solutes during quench. Solute data for higher pressure quenched aqueous fluids and quartz-hosted vapor inclusions are presented in Tables 9–11. The data at pressures of 130 (Table 9), 140 (Table 10), and 145 (Table 11) MPa indicate that Na, K, and Fe were lost from the experimental aqueous fluid during quench. Silicate glass recovered from these experiments is optically and chemically homogeneous (Table 6) and lacks visible crystals. The calculated ASI values for silicate glass from experiments at 110 to 145 MPa overlap and, thus, the drop in salinity of quenched aqueous fluid is not a result of an increased concentration of alkali elements in the higher pressure melts.

The loss of solutes results in a bulk salinity that is far lower than that determined microthermometrically for quartz-hosted fluid inclusions (Tables 2–5) at the experimental *P-T* conditions. The microthermometry data are consistent with published data for the NaCl-KCl-H_2O. These data indicate that using a traditional cold-seal apparatus to quantify the Na, K, and Fe (and other metals) concentrations in quenched aqueous fluids at 800 °C and pressures greater than 110 MPa yields data that underestimate the actual metal concentrations at run conditions. Based on the strong agreement between the microthermometric data for fluid inclusions trapped at *P-T* run conditions with predictions from analogue systems, we suggest that the use of synthetic fluid inclusions to trap aqueous fluids presents the best method for quantifying fluid compositions at elevated pressure and temperature.

DISCUSSION

The success of using synthetic fluid inclusions to trap experimentally produced immiscible saline, aqueous fluids at elevated *P-T* conditions hinges on the ability to demonstrate that the measured solute load of the elements of interest (here: Na, K, Fe, and Au) represent equilibrium concentrations at the time of entrapment. Previous experimental studies have demonstratee the attainment of major- and minor-element equilibrium in H_2O-saturated felsic melts on timescales of 4 to 5 days (Carmichael and Mackenzie 1963; Thompson and Mackenzie 1967; Bailey et al. 1974; Bailey and Cooper 1978; Candela and Holland 1984; Scaillet and MacDonald 2001). This timescale is consistent with experimental durations in the current study. However, whereas our experiments hinged on the achievement of equilibrium between haplogranite melt, Au metal, aqueous vapor, and brine,

TABLE 8. Solute data for quenched aqueous fluids, quart-hosted and glass-hosted fluid inclusions at 800 °C, 100 and 110 MPa

Run no.	Run duration (hours)	Analytical method	No. of fluid inclusions analyzed	Final* wt% NaCl eq.	Na† µg/g (±2σ)	K† µg/g (±2σ)	Fe† µg/g (±2σ)	Au‡ µg/g (±2σ)
Quenched aqueous fluid from 110 MPa experiments								
60	168	AAS	NA§	NA§	6125 ± 850	6450 ± 1250	3025 ± 275	ND‖
61	480	AAS	NA§	NA§	6600 ± 1100	5725 ± 975	3250 ± 450	ND‖
62	275	AAS	NA§	NA§	6550 ± 1500	5825 ± 1050	2900 ± 350	ND‖
Quartz-hosted vapor fluid inclusions from 110 MPa experiments								
60	168	LA-ICPMS	6	2.1 – 2.4	5900 ± 1150	5700 ± 875	3200 ± 1400	6 ± 3
61	480	LA-ICPMS	8	2.1 – 2.4	5700 ± 900	6250 ± 1350	2650 ± 1100	4 ± 2
62	275	LA-ICPMS	4	2.1 – 2.4	5100 ± 1300	5450 ± 650	3350 ± 1350	5 ± 3
Quartz-hosted brine fluid inclusions from 110 MPa experiments								
60	168	LA-ICPMS	7	57.1 – 59.5	136 000 ± 11 500	157 000 ± 14 500	63 500 ± 7500	32 ± 9
61	480	LA-ICPMS	5	57.2 – 59.0	144 000 ± 15 000	141 000 ± 17 000	67 000 ± 5000	31 ± 11
62	275	LA-ICPMS	7	57.1 – 59.5	141 000 ± 9000	151 000 ± 12 500	61 000 ± 6500	28 ± 7

* The range of wt% NaCl eq. values for synthetic vapor and brine fluid inclusions determined by microthermometry.
† These data were originally published in Simon et al. (2004).
‡ These data were originally published in Simon et al. (2005).
§ NA = not applicable.
‖ ND = not determined.

TABLE 9. LA-ICPMS data for quenched aqueous fluids and quartz-hosted fluid inclusions at 800 °C and 130 MPa

Run no.	Run duration (hours)	Analytical method	No. of fluid inclusions analyzed	Final* wt% NaCl eq.	Na† µg/g (±2σ)	K† µg/g (±2σ)	Fe† µg/g (±2σ)	Au‡ µg/g (±2σ)
Quenched aqueous fluid from 130 MPa experiments								
40	239.5	AAS	NA§	NA§	3700 ± 450	5700 ± 850	3850 ± 600	ND‖
52	275	AAS	NA§	NA§	4100 ± 500	4600 ± 700	4000 ± 450	ND‖
55	306.5	AAS	NA§	NA§	4600 ± 650	4900 ± 1100	4550 ± 500	ND‖
Quartz-hosted vapor fluid inclusions from 130 MPa experiments								
40	239.5	LA-ICPMS	6	2.1 – 2.4	9200 ± 1300	15100 ± 1950	9400 ± 1150	4.0 ± 1.5
52	275	LA-ICPMS	8	2.1 – 2.4	10 700 ± 1450	12900 ± 2100	9100 ± 1500	3.5 ± 2.0
55	306.5	LA-ICPMS	4	2.1 – 2.4	8500 ± 1600	14300 ± 1800	11500 ± 2200	4.5 ± 2.0
Quartz-hosted brine fluid inclusions from 130 MPa experiments								
40	239.5	LA-ICPMS	7	57.1 – 59.5	115 000 ± 12 000	121 000 ± 9100	68 500 ± 8500	31 ± 7
52	275	LA-ICPMS	5	57.2 – 59.0	105 000 ± 7500	141 000 ± 17 000	82 000 ± 9500	27 ± 9
55	306.5	LA-ICPMS	7	57.1 – 59.5	111 500 ± 14 000	127 000 ± 16 000	63 000 ± 8000	29 ± 5

* The range of wt% NaCl eq. values for synthetic vapor and brine fluid inclusions determined by microthermometry.
† These data were originally published in Simon et al. (2004).
‡ These data were originally published in Simon et al. (2005).
§ NA = not applicable.
‖ ND = not determined.

the ultimate goal of our experimental design was to produce a fully equilibrated vapor + brine assemblage that would migrate into pre-existing microfractures in quartz cores *before* crack self-healing. Thus, the success of our experimental technique deals with the competition between establishing bulk-chemical equilibrium within the charge and the rate at which quartz cracks heal.

Crack healing occurs most likely by local diffusion of SiO_2 from one part of the quartz crystal to another through the aqueous fluid that fills the crack. Brantley (1992) reported that quartz microfractures, at 200 MPa and 600 °C in the presence of NaCl-H_2O fluids, undergo self-healing of approximately 50% of the length of a given fracture on a timescale of 5 hours. The data Brantley collected at pressures higher and temperatures lower than those in the current study. Teinturier and Pironon (2003) trapped fluid inclusions in synthetic and natural quartz microfractures as the temperature was decreased isobarically, from 400 to 300 °C, at 40 MPa, over 20 days. They used microthermometrically determined salinities of fluid inclusions to estimate the healing time of individual cracks. Their data indicate that a NaCl-H_2O fluid requires six days to equilibrate with natural quartz. Furthermore, they suggest that crack healing can occur in the absence of an external silica supply although a low silica supply hinders crack healing. Considering that our experiments contained abundant silica, the rate of healing is hypothesized to be controlled predominantly by bulk-chemical equilibrium among the quartz chip, the silicate melt, and the silica-transporting aqueous fluids, both vapor and brine, that percolate through the cracks. These data sets suggest that crack healing occurs on a slow enough time scale to permit entrapment of equilibrated aqueous fluids. We note that the current study involved aqueous fluids with a low bulk salinity in experimental setup 2. The solubility of SiO_2 is lower in vapor-type fluids (Fournier and Potter 1982) and it is possible that increased solubility of SiO_2 in higher salinity fluids may promote faster rates of crack healing. However, the data from higher pressures, and correspondingly higher salinities, reported here suggest that crack healing is slow enough to permit entrapment of vapor and brine at bulk salinities up to 20 wt% NaCl eq. The vapor and brine inclusions trapped at 800 °C and 145 MPa have salinities (Table 5) that agree with extant experimental (Sourirajan and Kennedy 1962; Bodnar et al. 1985; Chou 1987a; Chou et al. 1992; Sterner et al. 1992) and thermodynamic (Anderko and Pitzer 1993) data. The previous discussion comparing Au-saturated quartz-hosted and glass-hosted brine inclusions evinces that brines with salinities approaching 60 wt% NaCl eq. do not promote crack healing prior to aqueous fluid equilibration. Thus, the experimental

TABLE 10. LA-ICPMS data for quenched aqueous fluids and quartz-hosted fluid inclusions at 800 °C and 140 MPa

Run no.	Run duration (hours)	Analytical method	No. of fluid inclusions analyzed	Final* wt% NaCl eq.	Na† µg/g (±2σ)	K† µg/g (±2σ)	Fe† µg/g (±2σ)	Au‡ µg/g (±2σ)
Quenched aqueous fluid from 140 MPa experiments								
47	250	AAS	NA§	NA§	14 000 ± 1650	15 750 ± 1900	13 300 ± 1450	ND‖
49	325	AAS	NA§	NA§	11 750 ± 1300	14 000 ± 1150	12 000 ± 1700	ND‖
Quartz-hosted vapor fluid inclusions from 140 MPa experiments								
47	250	LA-ICPMS	6	2.1 – 2.4	14 900 ± 2200	29 200 ± 4100	21 000 ± 2100	31 ± 12
49	325	LA-ICPMS	8	2.1 – 2.4	19 800 ± 3300	25 000 ± 3700	19 500 ± 2700	25 ± 6
Quartz-hosted brine fluid inclusions from 140 MPa experiments								
47	250	LA-ICPMS	7	42.3 – 44.1	79 500 ± 13 000	114 000 ± 11 000	66 000 ± 9500	44 ± 13
49	325	LA-ICPMS	5	42.1 – 44.0	83 500 ± 10 500	107 000 ± 13 000	79000 ± 11 000	37 ± 11

* The range of wt% NaCl eq. values for synthetic vapor and brine fluid inclusions determined by microthermometry.
† These data were originally published in Simon et al. (2004).
‡ These data were originally published in Simon et al. (2005).
§ NA = not applicable.
‖ ND = not determined.

TABLE 11. LA-ICPMS data for quenched aqueous fluids and quartz-hosted fluid inclusions at 800 °C and 145 MPa

Run no.	Run duration (hours)	Analytical method	No. of fluid inclusions analyzed	Final* wt% NaCl eq.	Na† µg/g (±2σ)	K† µg/g (±2σ)	Fe† µg/g (±2σ)	Au‡ µg/g (±2σ)
Quenched aqueous fluid from 145 MPa experiments								
59	265	AAS	NA§	NA§	22 750 ± 2500	36 300 ± 2950	25 800 ± 3300	ND‖
63	390	AAS	NA§	NA§	18 900 ± 2350	35 500 ± 4100	29 000 ± 3900	ND‖
Quartz-hosted vapor fluid inclusions from 145 MPa experiments								
59	265	LA-ICPMS	6	2.1–2.4	33 500 ± 3350	68 500 ± 11 500	39 500 ± 2700	33 ± 14
63	390	LA-ICPMS	8	2.1–2.4	28 500 ± 3100	64 500 ± 9400	41 000 ± 4200	41 ± 11
Quartz-hosted brine fluid inclusions from 145 MPa experiments								
59	265	LA-ICPMS	7	57.1–59.5	65 500 ± 13 000	105 500 ± 14 500	77 500 ± 11000	48 ± 14
63	390	LA-ICPMS	5	57.2–59.0	53 000 ± 6000	134 000 ± 21 000	66 000 ± 8500	53 ± 9

* The range of wt% NaCl eq. values for synthetic vapor and brine fluid inclusions determined by microthermometry.
† These data were originally published in Simon et al. (2004).
‡ These data were originally published in Simon et al. (2005).
§ NA = not applicable.
‖ ND = not determined.

technique described here is relevant to the study of the evolution of most high-temperature aqueous-fluid-saturated (vapor, brine, and vapor + brine) magmatic systems.

Another potential driving force for crack healing could be through a dissolution-precipitation mechanism caused by temperature gradients across the charge. We inhibited convectively driven premature self-healing of quartz microfractures and the formation of quartz overgrowths on the quartz core by minimizing the thermal gradient along the length of the charge and tilting the hot end of the vessel 10–12° up from horizontal. Teinturier and Pironon (2003) produced quartz overgrowths by slowly decreasing the temperature, at constant pressure, of their experiments. Their data suggest that a 5 °C temperature difference over a distance of about 50 µm decreases quartz solubility and results in quartz overgrowth formation. The temperature gradient in our experiments is ≤5 °C along the length of the 3 cm capsule. The hot spot corresponds to the middle of the capsule and the temperature profile across the capsule is 797 to 798 °C at the cold end, 801–802 °C at the hot end, and the mid-point of the capsule is 800 °C. The quartz cores are 1.5 cm long and are located inside the capsule such that the quartz core lies across the hot spot. The temperature profile across the quartz core is about 799 °C at the cold end and 801 °C at the hot end. Thus, the temperature gradients are 1.7 °C/cm across the length of the capsule and 1.3 °C/cm across the length of the quartz core. This minimal thermal gradient eliminates the potential for quartz overgrowths. Consistent solute loads of analyzed fluid inclusions from across the recovered quartz core further support a lack of chemical potential gradients within the charge. We did not analyze inclusions with intermediate salinities, which presumably are accidental mixtures of vapor plus brine trapped together in a given fluid inclusion population, or inclusions that suffered from post-entrapment necking down. The overgrowth of new quartz on the quartz core loaded into an experiment is evidence for an unacceptably high thermal gradient. It is critical that readers carefully evaluate data from experimental studies with reported, or inferred, strong chemical potential gradients.

We did not determine the Au concentrations of quenched aqueous fluids and/or glass-hosted vapor fluid inclusions. Consequently, demonstrating that the quartz-hosted vapor fluid inclusions contain equilibrium Au concentrations is not straightforward. The Au concentrations in quartz-hosted vapor inclusions increase from 5 ± 2 to 36 ± 11 with pressure from 110 to 145 MPa (Tables 9–11). This increase is consistent with the increased HCl concentration (and total salinity) of the vapor with increasing pressure. Additionally, the calculated partition coefficient for Au between vapor and brine, $D_{Au}^{v/b}$, increases systematically from 0.2 to 0.7 as pressure increases from 110 to 145 MPa (Simon et al. 2005). This increased partition coefficient value is consistent with the thermodynamic boundary condition that the value of $D_{Au}^{v/b}$ must become 1 at the critical pressure, on the order of 160 MPa for the NaCl-KCl-$FeCl_2$-HCl-$AuCl_2H$-H_2O system. The data reported here indicate that the brine contains an equilibrium Au concentration and, thus, we infer the Au behavior in the vapor, consistent with thermodynamic prediction, to suggest that the Au concentrations in quartz-hosted vapor fluid inclusions represent equilibrium.

The data presented in this study evince clearly that the chemical composition of fluids in quartz microfractures at the time of self-healing represents equilibrium conditions as long as the experimental set-up is well constrained (i.e., minimal thermal and chemical potential gradients are mandatory). Hence, by applying careful selection criteria, synthetic fluid inclusions in experiments with low thermal gradients across the charge provide a reasonable estimate of fluid composition at *PTX*. Any synthetic fluid inclusion data should be accompanied by statements concerning thermal gradients in the charge. Otherwise, the data should be considered suspect. Clearly, details of the experimental technique are critical for the proper interpretation of any subsequent analyses of fluid inclusions. In our view, overgrowths on quartz indicate that thermal gradients may be too high, causing significant uncertainties in temperature and premature healing of quartz fractures.

Application to ore deposit evolution

The application of our experimental technique to quantifying the thermodynamics of vapor + brine nucleation and concomitant metal partitioning systematics clearly can be seen in the proposed fluid evolution history of ore deposits such as the Big Gossan Deposit, Ertsberg District, Irian Jaya (Meinert et al. 2003), Bajo de la Alumbrera, Argentina (Ulrich et al. 2001), the Bismarck skarn deposit, Mexico (Baker and Lang 2003; Baker et al. 2004), and Bingham, Utah (Landtwing et al. 2005). Although the specific *PTX* pathways followed in these deposits differ, they share the similar characteristic of having been vapor + brine saturated owing to boiling of an early exsolved supercritical aqueous fluid. The supercritical fluid (2–10 wt% NaCl eq.) becomes unstable relative to coexisting brine and vapor as the aqueous fluid experiences decreasing *P-T* conditions and intersects the solvus. Metal partitioning between the vapor and brine is controlled by the fractionation of ligands between the two immiscible phases. Chloride is the dominant anion in the brine and, thus, all chloride-complexed metals are *predicted* to fractionate preferentially into the brine. SO_2, H_2S, and HCl are fractionated into the vapor (Candela and Piccoli 1995; Scaillet et al. 1998; Keppler 1999) and, thus, metals that prefer complexation with these bases are preferentially partitioned into the vapor phase. Some boiling assemblages (i.e., $D_{Au}^{v/b} \approx 39$ in the Grasberg high grade Cu-Au zone; Heinrich et al. 1999) preserve evidence that soft metals such as Au may prefer complexation with the reduced soft ligand HS^- (e.g., AuHS°, Seward 1991; Benning and Seward 1996; Stefánsson and Seward 2004) and fractionate into the vapor phase relative to the brine. In other deposits, there is no observed vapor fractionation of Au (e.g., $D_{Au}^{v/b} \approx 0.7$ in the Bajo de la Alumbrera magnetite-rich core to potassic Cu-Au ore; Ulrich et al. 1999). The mass ratios of H_2S/Cl, H_2S/SO_2, and HCl concentration of the evolving fluids are most likely responsible for the fractionation of Au (and other metals such as Cu, As) between the vapor and brine. As such, experiments in multi-phase fluid systems performed at controlled temperature, pressure, H_2S/Cl, H_2S/SO_2, and pH conditions offer the only possibility of constraining the thermodynamic controls responsible for the fractionation trends in boiling fluid inclusion assemblages. Understanding these controls is fundamental to advancing our knowledge of the evolution of magmatic-hydrothermal ore systems, as well as other igneous and metamorphic systems saturated with multi-phase aqueous fluids.

Acknowledgments

This work was partially supported by National Science Foundation grants: EAR 0309967 (PAC and PMP), EAR 9909576 (PAC and PMP), and EAR 0125805 (PAC and PMP); EAR 9810244 (PMP and others). We thank Mona Sirbescu, Robert Linnen, and Associate Editor Don Baker for their thorough and constructive reviews, which significantly strengthened the substance and conclusions of the paper. The Isotope Geochemistry and Mineral Resources group at ETH acknowledges continued support from the Swiss National Science Foundation. ACS thanks the Department of Geoscience and College of Sciences at UNLV for a first-year reduced teaching load, which allowed him to write this manuscript.

References cited

Acosta-Vigil, A., London, D., Morgan, G.B., and Dewers, T.A., VI (2003) Solubility of excess alumina in hydrous granitic melts in equilibrium with peraluminous minerals at 700–800 °C and 200 MPa, and applications of the aluminum saturation index. Contributions to Mineralogy and Petrology, 146, 100–119.

Allan, M.M., Yardley, B.W.D., Forbes, L.J., Shmulovich, K.I., Banks, D.A., and Shepherd, T.J. (2005) Validation of LA-ICP-MS fluid inclusion analysis with synthetic fluid inclusions. American Mineralogist, 90, 1767–1775.

Anderko, A. and Pitzer, K.S. (1993) Equation-of-state representation of phase equilibria and volumetric properties of the system NaCl-H_2O above 573 K. Geochimica et Cosmochimica Acta, 57, 1657–1680.

Anderson, G.M. and Burnham, C.W. (1965) The solubility of quartz in supercritical water. American Journal of Science, 263, 494–511.

Audétat, A. and Pettke, T. (2003) The magmatic-hydrothermal evolution of two barren granites: A melt and fluid inclusion study of the Rito del Medio and Cañada Pinabete plutons in northern New Mexico (USA). Geochimica et Cosmochimica Acta, 67, 97–121.

Audétat, A., Günther, D., and Heinrich, C.A. (1998) Formation of a magmatic hydrothermal ore deposit; insights in with LA-ICP-MS analysis of fluid inclusions. Science, 279, 2091–2094.

Audétat, A., Günther, D., and Heinrich, C.A. (2000) Magmatic-hydrothermal evolution in a fractionating granite: A microchemical study of the Sn-W-F-mineralized Mole Granite (Australia). Geochimica et Cosmochimica Acta, 64, 3373–3393.

Bailey, D.K. and Cooper, J.P. (1978) Comparison of the crystallization of pantelleritic obsidian under hydrous and anhydrous conditions. In W.S. MacKenzie, Ed., Progress in experimental petrology; fourth progress report of research supported by N.E.R.C. 1975–1978, p. 230–233.

Bailey, D.K., Cooper, J.P., and Knight, J.L. (1974) Anhydrous melting and crystallization of peralkaline obsidians. Bulletin of Volcanology, 38, 653–665.

Baker, T. and Lang, J.R. (2003) Reconciling fluid inclusion types, fluid processes, and fluid sources in skarns: an example from the Bismarck Deposit, Mexico. Mineralium Deposita, 38, 474–495.

Baker, T., Van Achterberg, E., Ryan, C., and Lang, J.R. (2004) Composition and evolution of ore fluids in a magmatic-hydrothermal skarn deposit. Geology, 32, 117–120.

Banks, D.A. and Yardley, B.W.D. (1992) Crush-leach analysis of fluid inclusions in small natural and synthetic samples. Geochimica Cosmochimica Acta, 56, 245–248.

Benning, L.G. and Seward, T.M. (1996) Hydrosulphide complexing of Au(I) in hydrothermal solutions from 150 to 400 °C and 500 to 1500 bars. Geochimica et Cosmochimica Acta, 60, 1849–1871.

Bodnar, R.J. and Sterner, S.M. (1985) Synthetic fluid inclusions in natural quartz. II. Application to *PVT* studies. Geochimica et Cosmochimica Acta, 49, 1855–1859.

——— (1987) Synthetic fluid inclusions. In G.C. Ulmer and H.L. Barnes, Eds., Hydrothermal experimental techniques, p. 423–457. John Wiley and Sons, New York.

Bodnar, R.J. and Vityk, M.O. (1994) Interpretation of microthermometric data for H_2O-NaCl fluid inclusions. In B. De Vivo and M.L. Frezzotti, Eds., Fluid Inclusions in Minerals, Methods and Applications, p. 117–130. Virginia Polytechnic Institute, Blacksburg.

Bodnar, R.J., Burnham, C.W., and Sterner, S.M. (1985) Synthetic fluid inclusions in natural quartz. III. Determination of phase equilibrium properties in the system H_2O-NaCl to 1000 °C and 1500 bars. Geochimica et Cosmochimica Acta, 49, 1861–1873.

Brantley, S.L. (1992) The effect of fluid chemistry on quartz microcrack lifetimes. Earth and Planetary Science Letters, 113, 145–56.

Candela, P.A. (1990) Theoretical constraints on the chemistry of the magmatic aqueous phase. In H.J. Stein and J.L. Hannah, Eds., Ore-bearing Granite Systems; Petrogenesis and mineralizing processes. Geological Society of America Special Paper, 246, 11–20.

Candela, P.A. and Holland H.D. (1984) The partitioning of copper and molybde-

num between silicate melts and aqueous fluids. Geochimica et Cosmochimica Acta, 48, 373–380.
Candela, P.A. and Piccoli, P.M. (1995) Model ore-metal partitioning from melts into vapor and vapor/brine mixtures. In J.F.H. Thompson, Ed., Magmas, Fluids, and Ore Deposits. Mineralogical Association of Canada Short Course, 23, 101–128.
Carmichael, I.S.E. and MacKenzie, W.S. (1963) Feldspar-liquid equilibria in pantellerites: an experimental study. American Journal of Science, 261, 382–396.
Charles, R.W. and Vidale, R. (1982) Temperature calibration of a new rapid quench vessel. American Mineralogist, 67, 175–179.
Chou, I.C. (1987a) Phase relations in the system NaCl-KCl-H_2O: III, Solubilities of halite in vapor-saturated liquids above 445 °C and redetermination of phase equilibrium properties in the system NaCl-H_2O to 1000 °C and 1500 bars. Geochimica et Cosmochimica Acta, 51, 1965–1975.
——— (1987b) Oxygen buffer hydrogen sensor techniques at elevated pressures and temperatures. In G.C. Ulmer and H.L. Barnes, Eds., Hydrothermal Experimental Techniques, p. 61–99. Wiley, New York.
Chou, I.C. and Eugster, H.P. (1977) Solubility of magnetite in supercritical chloride solutions. American Journal of Science, 277, 1296–1314.
Chou, I.-M., Sterner, S.M., and Pitzer, K.S. (1992) Phase relations in the system NaCl-KCl-H_2O: IV. Differential thermal analysis of the sylvite liquidus in the KCl-H_2O binary, the liquidus in the NaCl-KCl-H_2O ternary, and the solidus in the NaCl-KCl binary to 2 kb pressure, and a summary of experimental data for thermodynamic-*PTX* analysis of solid-liquid equilibria at elevated *P-T* conditions. Geochimica et Cosmochimica Acta, 56, 2281–2293.
Eggins, S.M., Kinsley, L.P.J., and Shelley, J.M.G. (1998) Deposition and element fractionation processes during atmospheric pressure laser sampling for analysis by ICP-MS. Applied Surface Science, 129, 278–286.
Fournier, R.O. and Potter, R.W., III (1982), An equation correlating the solubility of quartz in water from 25 °C to 900 °C at pressures up to 10,000 bars. Geochimica et Cosmochimica Acta, 46, 1969–1973.
Frank, M.R., Candela, P.A., Piccoli, P.M., and Glascock, M.D. (2002) Gold solubility, speciation, and partitioning as a function of HCl in the brine-silicate melt-metallic gold system at 800 °C and 100 MPa. Geochimica et Cosmochimica Acta, 66, 3719–3732
Frantz, J.D. and Popp, R.K. (1979) Mineral-solution equilibria. I. An experimental study of completing and thermodynamic properties of aqueous $MgCl_2$ in the system MgO-SiO_2-H_2O-HCl. Geochimica et Cosmochimica Acta, 43, 1223–1239.
Gagnon, J.E., Samson, I.M., Fryer, B.J., and Williams-Jones, A.E. (2004) The composition and origin of hydrothermal fluids in a NYF-type granitic pegmatite, South Platte District, Colorado: evidence from LA-ICP-MS analysis of fluorite- and quartz-hosted fluid inclusions. Canadian Mineralogist, 42, 1331–1355.
Glascock M. D. (1998) Activation analysis. In Z.B. Alfassi, Ed., Instrumental Multi-Element Chemical Analysis, p. 93–150. Kluwer Academic Publishers, Dordrecht.
Günther, D. and Heinrich, C.A. (1999) Enhanced sensitivity in laser ablation-ICP-mass spectrometry using helium-argon mixtures as aerosol carrier—Plenary lecture. Journal of Analytical Atomic Spectrometry, 14(9), 1363–1368.
Günther, D., Frischknecht, R., Heinrich, C.A., and Kahlert, H.J. (1997) Capabilities of an Argon fluoride 193 nm Excimer laser ablation inductively coupled plasma mass spectrometry microanalysis of geological materials. Journal of Analytical and Atomic Spectroscopy, 12, 939–944.
Günther, D., Audétat, A., Frischknecht, A., and Heinrich, C.A. (1998) Quantitative analysis of major, minor, and trace elements in fluid inclusions using laser ablation-inductively coupled plasma mass spectrometry. Journal of Analytical and Atomic Spectroscopy, 13, 263–270.
Halter, W., Pettke, T., and Heinrich, C.A. (2002) The origin of Cu/Au ratios in porphyry type oredeposits. Science, 296, 1844–1896.
Hanley, J.J., Mungall, J.E., Pettke, T., Spooner, E.T.C., and Bray, C.J. (2005) Ore metal redistribution by hydrocarbon-brine and hydrocarbon-halide melt phases, North Range footwall of the Sudbury Igneous Complex, Ontario, Canada. Mineralium Deposita, 40, 237–256.
Heinrich, C.A., Ryan, C.G., Mernagh, T.P., and Eadington, P.J. (1992) Segregation of ore metals between magmatic brine and vapor. Economic Geology, 87, 1566–1583.
Heinrich, C.A., Günther, D., Audétat, A., Ulrich, T., and Frischknecht, R. (1999) Metal fractionation between magmatic brine and vapor, determined by microanalysis of fluid inclusions. Geology, 27, 755–758.
Heinrich, C.A., Pettke, T., Halter, W.E., Aigner-Torres, M., Audétat, A., Günther, D., Hattendorf, D., Bleiner, D., Guillong, M., and Horn, I. (2003) Quantitative multi-element analysis of minerals, fluid and melt inclusions by Laser-Ablation Inductively-Coupled-Plasma Mass Spectrometry. Geochimica et Cosmochimica Acta, 67, 3473–3497.
Hemley, J.J., Cygan, G.L., Fein, J.B., Robinson, G.R., and d'Angelo, W.M. (1992) Hydrothermal ore-forming processes in the light of studies in rock-buffered systems: I. Iron-copper-zinc-lead sulfide solubility relations. Economic Geology, 87, 23–24.
Kamenetsky, V.S., Achterberg, E., Ryan, C.G., Naumov, V.B., Mernagh, T.P., and Davidson, P. (2002) Extreme chemical heterogeneity of granite-derived hydrothermal fluids: An example from inclusions in a single crystal of miarolitic quartz. Geology, 30, 459–462.
Keppler, H. (1999) Experimental evidence for the source of excess sulfur in explosive volcanic eruptions. Science, 284, 1652–1654.
Klemm, L., Pettke, T., Graeser, S., Mullis, J., and Kouzmanov, K. (2004) Fluid chemistry and evolution of Pb ± Ag mineralisation in the Bimetal, central Alps. Schweizerische Mineralogisch Petrographische Mitteilungen, 84, 189–212.
Korzhinskiy, M.A. (1987) The solubility of corundum in an HCl fluid and forms taken by Al. Geochemistry International, 24, 105–109.
Kostova, B., Pettke, T., Driesner, T., Petrov, P., and Heinrich, C.A. (2004) LA-ICP-MS study of fluid inclusions in quartz from the Yuzhna Petrovitsa deposit, Madan ore field, Bulgaria. Schweizerische Mineralogisch Petrographische Mitteilungen, 84, 25–36.
Kovalenko, N.I., Ryzhenko, B.N., Barsukov, V.L., Klintsova, A.P., Velyukhanova, T.K., Volynets, M.P., and Kitayeva, L.P. (1986) The solubility of cassiterite in HCl and HCl + NaCl (KCl) solutions at 500 °C and 1000 atm under fixed redox conditions. Geochemistry International, 23, 66–78.
Landtwing, M.R. and Pettke, T. (2005) Relationships between SEM-cathodoluminescence response and trace-element composition of hydrothermal vein quartz. American Mineralogist, 90, 122–131.
Landtwing, M.R., Pettke, T., Halter, W.E., Heinrich, C.A., Redmond, P.B., Einaudi, M.T., and Kunze, K. (2005) Causes for Cu-Fe-sulfide deposition in the Bingham porphyry Cu-Au-Mo deposit, Utah: combined SEM-cathodoluminescence petrography and LA-ICPMS analysis of fluid inclusions. Earth and Planetary Science Letters 235, 229–243.
Liu, W., McPhail, D.C., and Brugger, J. (2000) The solubility of cuprite in aqueous chloride and acetate solutions between 50 °C and 250 °C. EMPG VIII, 8th International Symposium on Experimental Mineralogy, Petrology and Geochemistry, Bergamo, Italy.
Manning, C.E. (1994) The solubility of quartz in H_2O in the lower crust and upper mantle. Geochimica et Cosmochimica Acta, 58, 4831–4839.
——— (2004) The chemistry of subduction-zone fluids. Earth and Planetary Science Letters, 223, 1–16.
Manning, C.E. and Boettcher, S.L. (1994) Rapid-quench hydrothermal experiments at mantle pressures and temperatures. American Mineralogist, 79, 1153–1158.
Mavrogenes, J.A., Bodnar, R.J., Anderson, A.J., Bajt, S., Sutton, S.R.. and Rivers, M.L. (1995) Assessment of the uncertainties and limitations of quantitative elemental analysis of individual fluid inclusions using synchrotron X-ray fluorescence (SXRF). Geochimica et Cosmochimica Acta, 59, 3987–3995.
McMahon, G., Cabri, L.J., Hames, A., Hervig, R.L., and Williams, P. (2000) Trace analyses of Pt and Au using primary ion beams of Cs+ and K+: A comparative study. In A. Benninghoven, P. Bertrand, H.-N. Migeon, and H.W. Werner, Eds., Secondary Ion Mass Spectrometry, SIMS XII, p. 131–134. Elsevier, Amsterdam.
Meinert, L.D., Hedenquist, J.W., Satoh, H., and Matsuhisa, Y. (2003) Formation of anhydrous and hydrous skarn in Cu-Au ore deposits by magmatic fluids. Economic Geology, 98, 147–156.
Morgan, G.B., VI and London, D. (1996) Optimizing the electron microprobe analysis of hydrous alkali aluminosilicate glasses. American Mineralogist, 81, 1176–1185.
Newton, R.C. and Manning, C.E. (2000) Quartz solubility in concentrated aqueous NaCl solutions at deep crust-upper mantle metamorphic conditions: 2–15 kbar and 500–900 °C. Geochimica Cosmochimica Acta, 64, 2993–3005.
——— (2002) Experimental determination of calcite solubility in H_2O-NaCl solutions at deep crust/upper mantle pressures and temperatures: implications for metasomatic processes in shear zones. American Mineralogist, 87, 1401–1409.
Pearce, N.J.G., Perkins, W.T., Westgate, J.A., Gorton, M.P., Jackson, S.E., Neal, C.R., and Chenery, S.P. (1997) A compilation of new and published major and trace element data for NIST SRM 610 and NIST 612 glass reference materials. Geostandards Newsletter, 21, 115–144.
Pettke, T., Kouzmanov, K., Halter, W., and Heinrich, C.A. (2003) The chemical evolution of melts and fluids associated with the porphyry-type copper-gold-PGE-deposit at Elatsite, Bulgaria. Geological Society of America Abstracts with Programs, 35(6), 357.
Pettke, T., Halter, W.E., Webster, J.D., Aigner-Torres, M., and Heinrich, C.A. (2004) Accurate quantification of melt inclusion chemistry by LA-ICPMS: a comparison with EMP and SIMS and advantages and possible limitations of these methods. Lithos, 78(4), 333–361.
Popp, R.K. and Frantz, J.D. (1980) Mineral solution equilibria-III. The system Na_2O-Al_2O_3-SiO_2-H_2O-HCl. Geochimica et Cosmochimica Acta, 47, 1029–1037.
Redmond, P.B., Einaudi, M.T., Inan, E.E., Landtwing, M.R., and Heinrich, C.A. (2004) Copper deposition by fluid cooling in intrusion-centered systems: New insights from the Bingham porphyry ore deposit, Utah. Geology, 32, 217–220.
Roedder, E. (1984) Fluid Inclusions (Monograph), 12, 644 p. Reviews in Mineral-

ogy, Mineralogical Society of America, Chantilly, Virginia.
Ryan, C.G., Heinrich, C.A., and Mernagh, T.P. (1993) PIXE microanalysis of fluid inclusions and its application to study of ore metal segregation between magmatic brine and vapor. Nuclear Instrumental Methods, B77, 463–471.
Ryan, C.G., Jamieson, D.N., Griffin, W.L., Cripps, G., and Szymanski, R. (2001) The new CSIRO-GEMOC nuclear microprobe: First results, performance and recent applications. Nuclear Instrumental Methods, B181, 12–19.
Scaillet, B. and MacDonald, R. (2001) Phase relations of peralkaline silicic magmas and petrogenetic implications. Journal of Petrology, 42, 825–845.
Scaillet, B., Clemente, B., Evans, B.W., and Pichavant, M. (1998) Redox control of sulfur degassing in silicic magmas. Journal of Geophysical Research, 103, 23937–23949.
Scambelluri, M., Müntener, O., Ottolini, L., Pettke, T., and Vannucci, R. (2004a) The rate of B, Cl and Li in the subducted oceanic mantle and the antigorite breakdown fluids. Earth and Planetary Science Letters, 220, 131–137.
Scambelluri, M., Fiebig, J., Malaspina, N., Muntener, O., and Pettke, T. (2004b) Serpentinite subduction: Implications for fluid processes and trace-element recycling. International Geology Review, 46(7), 595–613.
Seward, T.M. (1991) The hydrothermal geochemistry of gold. In R.P. Foster, Ed., Gold Metallogeny and exploration, p. 37–62. Blackie and Son, Glasgow.
Shepherd, T.J. and Chenery, S.R. (1995) Laser ablation ICP-MS elemental analysis of individual fluid inclusions: an evaluation study. Geochimica et Cosmochimica Acta, 59, 3997–4007.
Simon, A.C. (2003) An experimental study to eludicate magnetite solubility and metal partitioning in a magnetite-silicate melt-vapor-brine-gold metal assemblage, 194 p. Ph.D. Dissertation, University of Maryland.
Simon, A.C., Frank, M.R., Pettke, T., Candela, P.A., Heinrich, C.A., and Piccoli, P.M. (2003a) Experiments using pre-fractured quartz to trap volatile phases: Can we believe the data? GSA 2003 Annual Meeting, Paper No. 135-3.
Simon, A.C., Pettke, T., Candela, P.A., Piccoli, P.M., and Heinrich, C. (2003b) Experimental determination of gold solubility in haplogranite melt and magnetite: constraints on magmatic gold budgets. American Mineralogist, 88, 1644–1651.
Simon, A.C., Pettke, T., Candela, P.A., Piccoli, P.M., and Heinrich, C. (2004) Magnetite solubility and iron transport in magmatic-hydrothermal environments. Geochimica Cosmochimica Acta, 68, 4905–4914.
Simon, A.C., Frank, M., Pettke, T., Candela, P.A., Piccoli, P.M., and Heinrich, C. (2005) Gold partitioning in melt-vapor-brine systems. Geochimica Cosmochimica Acta, 69, 3321–3335.
Sourirajan, S. and Kennedy, G.C. (1962) The system NaCl-H_2O at elevated temperatures and pressures. American Journal of Science, 260, 115–141.
Stefánsson, A. and Seward, T.M. (2003) Stability of chloridogold(I) complexes in aqueous solution from 300 to 600 °C and from 500 to 1800 bar. Geochimica et Cosmochimica Acta, 23, 4559–4576.
——— (2004) Gold(I) complexing in aqueous sulphide solutions to 500 °C and 500 bar. Geochimica et Cosmochimica Acta, 68, 4121–4143.
Sterner, S.M. and Bodnar, R.J. (1984) Synthetic fluid inclusions in natural quartz: I. Compositional types synthesized and applications to experimental geochemistry. Geochimica et Cosmochimica Acta, 48, 2659–2668.
Sterner, S.M., Chou, I.-M., Downs, R.T., and Pitzer, K.S. (1992) Phase relations in the system NaCl-KCl-H_2O: V. Thermodynamic-*PTX* analysis of solid-liquid equilibria at high temperatures and pressures. Geochimica et Cosmochimica Acta, 56, 2295–2309.
Tagirov, B.R., Zoo, A.V., and Kingie, N.N. (1997) Experimental study of dissociation of HCl from 350 to 500 °C and from 500 to 2500 bars: Thermodynamic properties of HCl. Geochimica et Cosmochimica Acta, 61, 4267–4280.
Teinturier, S. and Pironon, J. (2003) Synthetic fluid inclusions as recorders of microfracture healing and overgrowth formation rates. American Mineralogist, 88, 1204–1208.
Thompson, R.N. and MacKenzie, W.S. (1967) Feldspar-liquid equilibria in peralkaline acid liquids: an experimental study. American Journal of Science, 265, 714–734.
Ulrich, T., Günther, D., and Heinrich, C.A. (1999) Gold concentrations of magmatic brines and the metal budget of porphyry copper deposits. Nature, 399, 676–679.
——— (2001) Evolution of a porphyry Cu-Au deposit, based on LA-ICP-MS analysis of fluid inclusions: Bajo de la Alumbrera, Argentina. Economic Geology, 97 (2002 reprint), 1888–1920.
Vanko, D.A., Bodnar, R.J., and Sterner, S.M. (1988) Synthetic fluid inclusions: VIII. Vapour saturated halite solubility in part of the system NaCl-CaCl2-H_2O, with applications to fluid inclusions from oceanic hydrothermal systems. Geochimica et Cosmochimica Acta, 52, 2451–2456.
Whitney, J.A., Hemley, J.J., and Simon, F.O. (1985) The concentration of iron in chloride solutions equilibrated with synthetic granite compositions: the sulfur-free system. Economic Geology, 80, 444–460.
Williams, T.J., Candela, P.A., and Piccoli, P.M. (1995) The partitioning of copper between silicate melts and two-phase aqueous fluids: An experimental investigation at kbar, 800 °C and 0.5 kbar, 850 °C. Contributions to Mineralogy and Petrology, 121, 388–399.
——— (1997) Hydrogen-alkali exchange between silicate melts and two-phase aqueous mixtures; an experimental investigation. Contributions to Mineralogy and Petrology, 128, 114–126.
Wood, S.A., Crerar, D.A., and Borcsik, M.P. (1987) Solubility of the assemblage pyrite pyrrhotite-magnetite-sphalerite-galena-gold-stibnite-bismuthinite-argentite-molybdenite in H_2O-NaCl-CO_2 solutions from 200 to 350 °C. Economic Geology Bulletin, Society of Economic Geologists, 82, 1867–1867.

MANUSCRIPT RECEIVED AUGUST 18, 2005
MANUSCRIPT ACCEPTED JULY 24, 2006
MANUSCRIPT HANDLED BY DON BAKER